Aluminum tri-isopropoxide as an alternative precursor for atomic layer deposition of aluminum oxide thin films

Fatemeh S. M. Hashemi, LiAo Cao, Felix Mattelaer, Timo Sajavaara, J. Ruud van Ommen, and Christophe Detavernier

Citation: Journal of Vacuum Science & Technology A **37**, 040901 (2019); doi: 10.1116/1.5093402
View online: https://doi.org/10.1116/1.5093402
View Table of Contents: https://avs.scitation.org/toc/jva/37/4
Published by the American Vacuum Society

Aluminum tri-isopropoxide as an alternative precursor for atomic layer deposition of aluminum oxide thin films

Fatemeh S. M. Hashemi,[1,a),b)] LiAo Cao,[2,a)] Felix Mattelaer,[2] Timo Sajavaara,[3] J. Ruud van Ommen,[1] and Christophe Detavernier[2]
[1]*Department of Chemical Engineering, Delft University of Technology, Delft 2629, The Netherlands*
[2]*Department of Solid State Sciences, Ghent University, Krijgslaan 281 S1, 9000 Gent, Belgium*
[3]*Department of Physics, University of Jyväskylä, P.O. Box 35, FIN-40014 Jyvaskyla, Finland*

(Received 20 February 2019; accepted 23 May 2019; published 8 July 2019)

Due to the safety challenges associated with the use of trimethylaluminum as a metal precursor for the deposition of alumina, different chemicals have been investigated over the years to replace it. The authors have investigated the use of aluminum tri-isopropoxide (TIPA) as an alternative alkoxide precursor for the safe and cost-effective deposition of alumina. In this work, TIPA is used as a stable Al source for atomic layer deposition (ALD) of Al_2O_3 when different oxidizing agents including water, oxygen plasma, water plasma, and ozone are employed. The authors have explored the deposition of Al_2O_3 using TIPA in ALD systems operating in vacuum and atmospheric pressure conditions. For thermal and plasma processes in vacuum ALD, a growth rate of 1.1–2 Å/cycle achieved over a range of 140–300 °C is shown. Film density, roughness, and composition have been tested using various characterization techniques confirming comparable film properties to the thermal ALD of trimethylaluminum and water. The thermal water process at atmospheric pressure ALD (AP-ALD) resulted in a growth rate of up to 1.1 Å/cycle with residual carbon below the XPS detection limit. AP-ALD on nanoparticles shows different growth modes on TiO_2 versus SiO_2 nanoparticle surfaces confirmed by transmission electron microscopy analysis. Using TIPA as an ALD precursor would open up the possibility for a safer and cost-effective process for deposition of Al_2O_3 in various applications. *Published by the AVS.* https://doi.org/10.1116/1.5093402

I. INTRODUCTION

Aluminum oxide thin films are widely used as encapsulation material,[1–3] barrier layer,[4,5] and dielectric film[6] due to their excellent chemical and thermal stability, high field strength, and high resistivity. In many cases, a thin layer of alumina coating is sufficient to provide these interesting properties, making atomic layer deposition (ALD) an ideal candidate for deposition of alumina. While ALD owes its initial popularity to the need for conformal nanocoatings in micro- and nanoelectronics, the unique advantages of thickness control and conformality of the ALD technique have inspired investigations into applications outside of the cleanroom, such as photovoltaics, powder coating, and flexible electronics. In recent years, reactor concepts and equipment have become available for large-area ALD.[7–9] Large-area coating has become enabled by continuous ALD processing or spatial ALD, both for photovoltaics, roll-to-roll and powder coating. The implementation of large-area ALD will increase precursor consumption with a factor of 100 for roll-to-toll applications and up to a factor of 10 000 for powder applications, as compared to the typical precursor consumption in state of the art tools for ALD in microelectronics fabrication.[10] This improvement will thus only be feasible if the precursors have a reasonable cost and are safe for use in large scale.

The most common process for ALD of alumina is its thermal deposition using trimethylaluminum (TMA) and water.[11–16] TMA has high volatility and thermal stability and is very reactive acting as an ideal precursor for the deposition of Al_2O_3 at various temperatures. However, TMA is pyrophoric, toxic, and corrosive. Moreover, when aiming to coat high surface areas such as nanoparticles, which typically have an area of over tens of m^2/g, over 10 mg of TMA per ALD cycle would be required making the process relatively expensive.[17] There have been many efforts to replace TMA with safer alternatives in ALD of alumina. These include the use of dimethylaluminum isopropoxide,[18,19] $[MeC(NiPr)_2]AlEt_2$,[20] aluminum trichloride,[6,21–24] triethylaluminum,[25] and dimethylaluminum chloride.[26] However, while these precursors are not pyrophoric they still rise safety, contamination, and cost issues when used at a large scale.

Alkoxide precursors are a safe alternative to alkyls. They exhibit moderate thermal stability and are cost-effective when needed to be produced in large amounts. Aluminum tri-isopropoxide (TIPA) has been used as both aluminum and oxygen source for deposition of alumina films through atomic layer deposition, chemical vapor deposition, and decomposition.[27–31] The alumina film deposition using TIPA was done at elevated temperatures (350–1000 °C), and the films displayed amorphous behaviour unless deposited or annealed at very high temperatures (above 1000 °C).[28,31] While TIPA has shown potential for deposition of alumina at elevated temperatures, no studies have explored the use of TIPA as an Al containing reagent (and not the oxidizer) for deposition of alumina in ALD. In order to deposit

[a)]F. S. M. Hashemi and L. Cao contributed equally to this work.
[b)]Author to whom correspondence should be addressed: f.s.minayehashemi@tudelft.nl

carbon-free alumina films at lower temperatures using TIPA, we propose both thermal and plasma-assisted ALD.

In this work, we have explored the deposition of Al_2O_3 using TIPA in vacuum and atmospheric pressure ALD systems. The deposition process has been studied both on planar substrates and on different nanoparticles to explore the feasibility of using TIPA for various purposes including large-scale applications. During thermal and plasma processes in vacuum ALD, we show a growth window of Al_2O_3 from 140 up to 300 °C. Growth rates achieved in the plasma process are comparable to the thermal ALD of TMA and water (1.1 Å/cycle). X-ray reflectivity (XRR) analysis confirms an increasing density of Al_2O_3 films when deposition temperature is increased. Scanning electron microscopy (SEM) and atomic force microscopy (AFM) show deposition of smooth films when TIPA is used as a precursor. X-ray photoelectron spectroscopy (XPS) studies confirm stoichiometric deposition of Al_2O_3 with carbon contamination below XPS detection limits. The thermal water process at atmospheric pressure ALD (AP-ALD) resulted in a growth rate of up to 1.1 Å/cycle. No growth was observed when ozone was used as the oxidizing agent under atmospheric pressure or vacuum conditions. Alumina deposition on nanoparticles via AP-ALD is confirmed via transmission electron microscopy (TEM) and energy dispersive x-ray (EDX) analysis. Some studies on chemical properties of TIPA report certain drawbacks associated with this precursor. These include precursor polymerization upon heating and cooling, changes in the precursor reactivity, and precursor decomposition.[29,32–36] Through the course of our experiments in vacuum and atmospheric pressure ALD systems, on flat substrates, and on nanoparticles, we did not encounter any issues with changes in the precursor reactivity. In the vacuum ALD system, no precursor decomposition was observed in the bubbler. In order to avoid precursor decomposition in the AP-ALD, the precursor was replaced after being heated in the bubbler for about 24 h. This work shows the possibility of a safe and scalable process for ALD of alumina using TIPA that can be adapted for various applications.

II. EXPERIMENT

ALD experiments were carried out in two different ALD systems: one operated under vacuum and one in atmospheric pressure. In the home-built vacuum-type ALD reactor, aluminum isopropoxide (TIPA) was used to deposit aluminum oxide films in combination with H_2O as the reactant. Both water and TIPA were stored in stainless steel bottles attached to the pump-type reactor.[37] The water bottle was kept at room temperature, and the line transferring the water vapor to the chamber was heated to 80 °C. The bottle containing TIPA was heated to 125 °C to generate enough precursor vapor, and the conveying line was heated to 130 °C to avoid precursor condensation. During the deposition, the wafer was placed on an evenly heated copper block and the temperature varied from 140 to 300 °C. The TIPA precursor vapor was carried into the reactor by Ar carrier gas. The pressure of the precursor pulse was controlled at 0.005 mbar while the turbo pump was running. Water, oxygen plasma, and water plasma were used as reactants. The plasma was generated in a fused quartz column wrapped by a copper coil on top of the chamber, which is connected to a 13.56 MHz RF generator (ENI GHW-12Z). By feeding oxygen and water vapor to the column at a pressure of 0.005 mbar, the remote plasma was set at 200 W and generated with an impedance matching network to minimize the reflected power. The saturation tests of precursor and reactants were performed at 150 °C.

The AP-ALD experiments were carried out in a home-built fluidized bed reactor operating at atmospheric pressure as described elsewhere.[38] The ALD chamber consists of a glass column (50 mm in internal diameter and 200 mm in height). The Al precursor contained in a stainless steel bubbler was heated and maintained at 125 °C. The stainless steel tubing connecting the bubbler and the reactor was maintained at 135 °C to avoid precursor condensation. Water was contained in a stainless steel bubbler and kept at room temperature. The line transferring water to the reaction column was kept at 130 °C. The reactor was heated by an infrared lamp placed parallel to the column with feedback control to maintain a constant temperature during ALD. The precursor was carried to the reactor column with a gas flow of 0.5 l min^{-1}. The ALD process consisted of sequential exposures of the Si substrates or nanoparticle powders to the Al precursor (5–240 s) and water or ozone (40 s), separated by a purging step (3–4 min) using nitrogen as an inert gas (N_2, 99.999 vol. %).

A. Materials

The substrates used for vacuum ALD were Si (100) wafers with native oxide and treated by oxygen plasma to remove surface contamination before deposition. Si (100) substrates used for AP-ALD were cleaned by UV/ozone for 5 min. The cleaned Si wafers contained about 1.5 nm of surface oxide.

Aeroxide P25 titanium oxide particles had a mean diameter of 32.7 nm, a specific area of 52.4 m^2/g, and a surface concentration of hydroxyl groups of 5.0 OH/nm^2. Hydrophilic fumed Aerosil OX 50 silica nanoparticles had a mean diameter of 40 nm, a specific area of 50 m^2/g, and an average SiOH density of 2.2 OH/nm^2. Both types of nanoparticles were purchased from Evonik Industries, and prior to the ALD deposition, they were sieved and heated overnight at 120 °C. Aluminum tri-isopropoxide (99%) was purchased from Sigma Aldrich and used without further purification.

B. Characterization

In the vacuum-type ALD setup, the aluminum oxide film growth rate was monitored *in situ* by spectroscopic ellipsometry (J.A. Woollam M-2000) using a Cauchy model for Al_2O_3. The parameters of the Cauchy model were modified by inputting the thickness of aluminum oxide films measured *ex situ* with XRR. XRR patterns, obtained by a Bruker D8 diffractometer using Cu Kα radiation, were analyzed by fitting simulated patterns to measured ones, yielding not only the film thickness but also the film density. SEM was

performed for surface imaging by an FEI Quanta 200F setup with a 10 keV electron beam energy. The surface morphology was determined by AFM on a Bruker Dimension Edge system operating in tapping mode in air. XPS was conducted using a Theta Probe system from Thermo Scientific using Al Kα x rays generated at 15 kV and focused to a spot size of 0.3 mm by an MXR1 monochromator gun to analyze the chemical composition of the films. Before XPS measurements, samples were cleaned with a short Ar pulse to remove adventitious carbon. Time-of-flight elastic recoil detection (tof-ERD) was performed using a home-built spectrometer and a 1.7 MV Pelletron accelerator in Jyväskylä.[39] The incident particle beam for these measurements consisted of 11.915 MeV $^{79}Br^{6+}$ ions at an incoming angle of 10° and a measuring angle of 31°, equaling a total scattering angle of 41°. The collected spectra were analyzed using in-house developed open-source software called POTKU.[40] The Al_2O_3 film thickness deposited via AP-ALD on Si was determined by *ex situ* spectroscopic ellipsometry (J.A. Woollam Co., Inc.) with a Cauchy dispersion model. XPS spectra on Si wafers after AP-ALD were measured on a K-Alpha Thermo Scientific scanning microprobe spectrometer using monochromatic Al Kα emission. TEM images on nanoparticles were obtained using a JEOL JEM 1400 with 120 kV beam voltage.

III. RESULTS AND DISCUSSION

In order to compare the physical properties of TIPA with TMA, we have calculated the vapor pressure of TIPA based on the thermogravimetric analysis measurements. The vapor pressure of these two precursors at temperatures ranging between 60 and 160 °C is in agreement with previously reported values (Fig. 1 in the supplementary material[62]).[37,41,42,62] While TIPA, with a melting point of 137 °C, shows a lower vapor pressure compared to TMA, it has a reasonable pressure (1.7–2.2 mbar) for ALD when heated at 125 °C. Precursor decomposition tests on a heated substrate at 400 °C indicated that a minimum bubbler temperature of 125 °C was required for the precursor to reach the ALD chamber. Thus, the bubbler temperature was kept at 125 °C. This temperature is also well below the decomposition temperature for TIPA.[29,37,41] We tested the precursor saturation for TIPA in the vacuum ALD setup using water, water plasma and oxygen plasma as the reactants. *In situ* ellipsometry results confirm that the precursor reaches saturation after 5 s pulse for all the cases [Fig. 1(a)] with the growth per cycle being the highest for the water process (2 Å/cycle) and similar for both plasma processes (1.1 Å/cycle). These growth per cycle are higher than or similar to the thermal TMA and water process (1.1 Å/cycle).[11,21] Increasing the precursor purge time at low operation temperatures did not affect this growth rate (Fig. 2 in the supplementary material[62]). No growth was observed when ozone was used as the counter reactant. Varying the reactant pulse time while keeping the precursor pulse 5 s shows that a 5 s pulse results in saturation of the reactant (Fig. 3 in the supplementary material[62]). Studies on the effect of the reaction temperature ranging from 140 to 300 °C show that the growth rate decreases from 1.8 Å/cycle

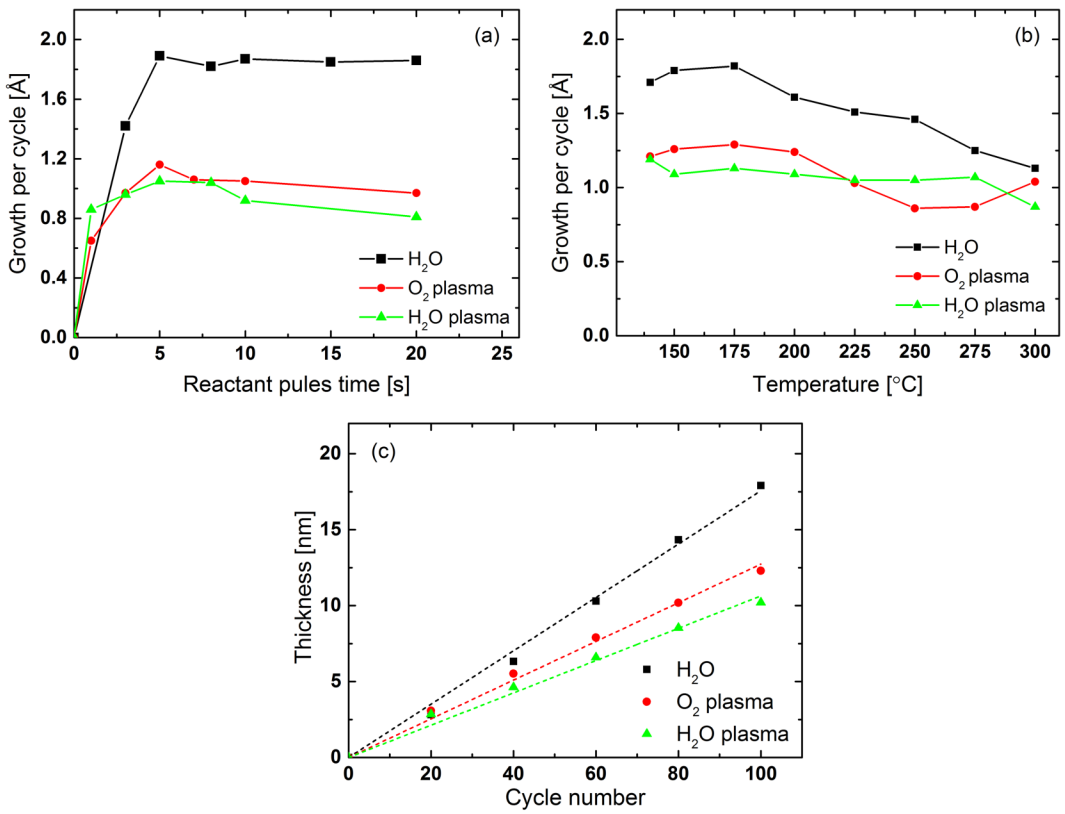

FIG. 1. (a) Saturation curve at 150 °C, (b) temperature window for TIPA pulse of 15 s, and (c) linear growth behavior of the vacuum ALD process on Si using water, water plasma, and O_2 plasma as reactants at 150 °C.

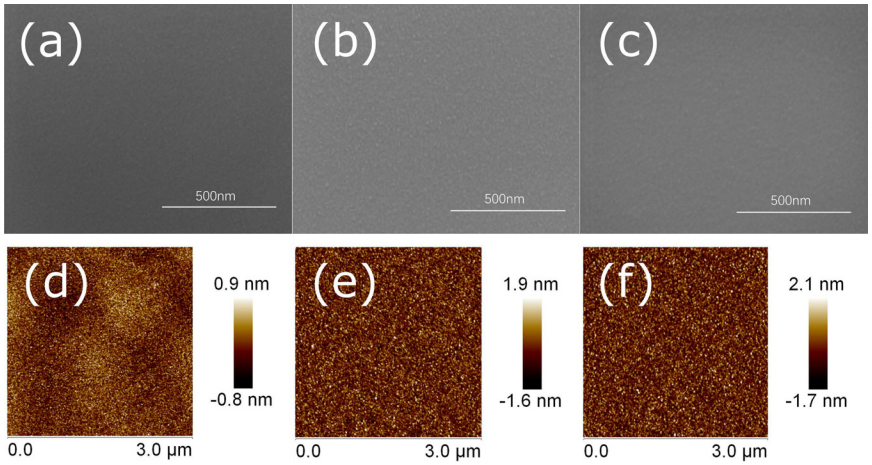

FIG. 2. SEM and AFM images of alumina films deposited at 150 °C using [(a) and (d)] O_2 plasma, [(b) and (e)] water plasma, and [(c) and (f)] water as the reactant.

(at 140 °C) down to 1.2 Å/cycle (at 300 °C) for the thermal water process in vacuum ALD [Fig. 1(b)]. Oxygen plasma and water plasma processes show a relatively steady growth per cycle of 1.1 ± 0.1 Å/cycle over the investigated temperature range [Fig. 1(b)]. Moreover, the film thickness increases linearly as a function of the number of ALD cycles, as confirmed by *in situ* ellipsometry [Fig. 1(c)]. Figure 1 confirms the expected ALD behavior of the TIPA reaction both in thermal and in plasma process.

To further investigate the quality of the films deposited via thermal and plasma ALD of TIPA, SEM and AFM studies were carried out on the films deposited at 150 °C using oxygen plasma [Figs. 2(a) and 2(d)], water plasma [Figs. 2(b) and 2(e)], and water [Figs. 2(c) and 2(f)] as the reactant. The results confirm the deposition of smooth, conformal, and uniform films. XPS analysis (Fig. 4 in the supplementary material[62]) shows stoichiometric alumina films deposited in the vacuum ALD process during both thermal and plasma processes. No residual carbon was detected by XPS.

The Al_2O_3 films obtained in this process show densities that are close to the bulk density of alumina (3.89 g/cm^3)[43]

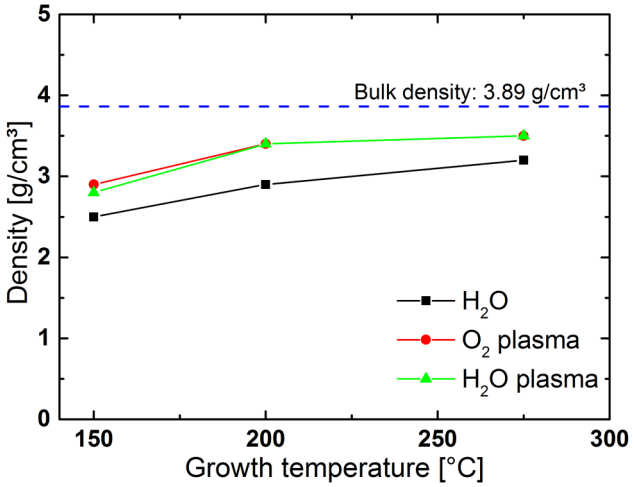

FIG. 3. Film densities for Al_2O_3 films (TIPA 15 s pulse, 100 cycles) deposited at different temperatures using O_2 plasma, water plasma, and water as the reactant.

when the films are deposited at higher temperatures (above 250 °C) (Fig. 3). Film densities are lower for the thermally deposited films using water and are higher when plasma ALD is applied (Fig. 3). The observed low density of alumina films deposited at 150 °C may be explained by an increase in the Al–O bond length at low temperatures as predicted by recent computational analysis.[44]

Furthermore, as the carbon content was below the detection limit of XPS, this lower-than-bulk density introduces the hypothesis of hydrogen incorporation into the samples, especially for the thermally grown films at lower temperatures.

Since XPS cannot detect hydrogen, ToF-ERD was used to determine the hydrogen content and to provide a more sensitive detection for light elements such as carbon and oxygen. Four samples were selected: thermal ALD using H_2O as a reactant at low temperature (150 °C) and high temperature (275 °C) and oxygen plasma-enhanced ALD at the same temperatures. Tof-ERD analysis confirmed the low carbon content from XPS. The thermal ALD films showed carbon contents of only 0.4 and 1.0 at. % for the high-temperature and low-temperature cases, respectively. The PE-ALD based films showed even lower carbon content, close to even the detection limit of ToF-ERD (<0.2 at. %) for this kind of thin films (Table I).

Furthermore, these four cases can be divided into two categories, based on their density: low-density films for the thermal process at low temperature and high-density films for the thermal process at high temperature and for the

TABLE I. Atomic concentrations in the central region of the deposited films, not taking into account interface effects at the surface or silicon interfaces, as calculated from the ToF-ERD measurements using POTKU software.

	O (at. %)	Al (at. %)	H (at. %)	C (at. %)
H_2O ALD, 150 °C	51 ± 3	24 ± 2	24 ± 2	1.0 ± 0.3
H_2O ALD, 275 °C	60 ± 3	37 ± 2	3.1 ± 0.3	0.4 ± 0.1
O_2 PE-ALD, 150 °C	60 ± 3	33 ± 2	6.1 ± 1.0	<0.2
O_2 PE-ALD, 275 °C	61 ± 4	35 ± 3	4.0 ± 1.0	<0.1

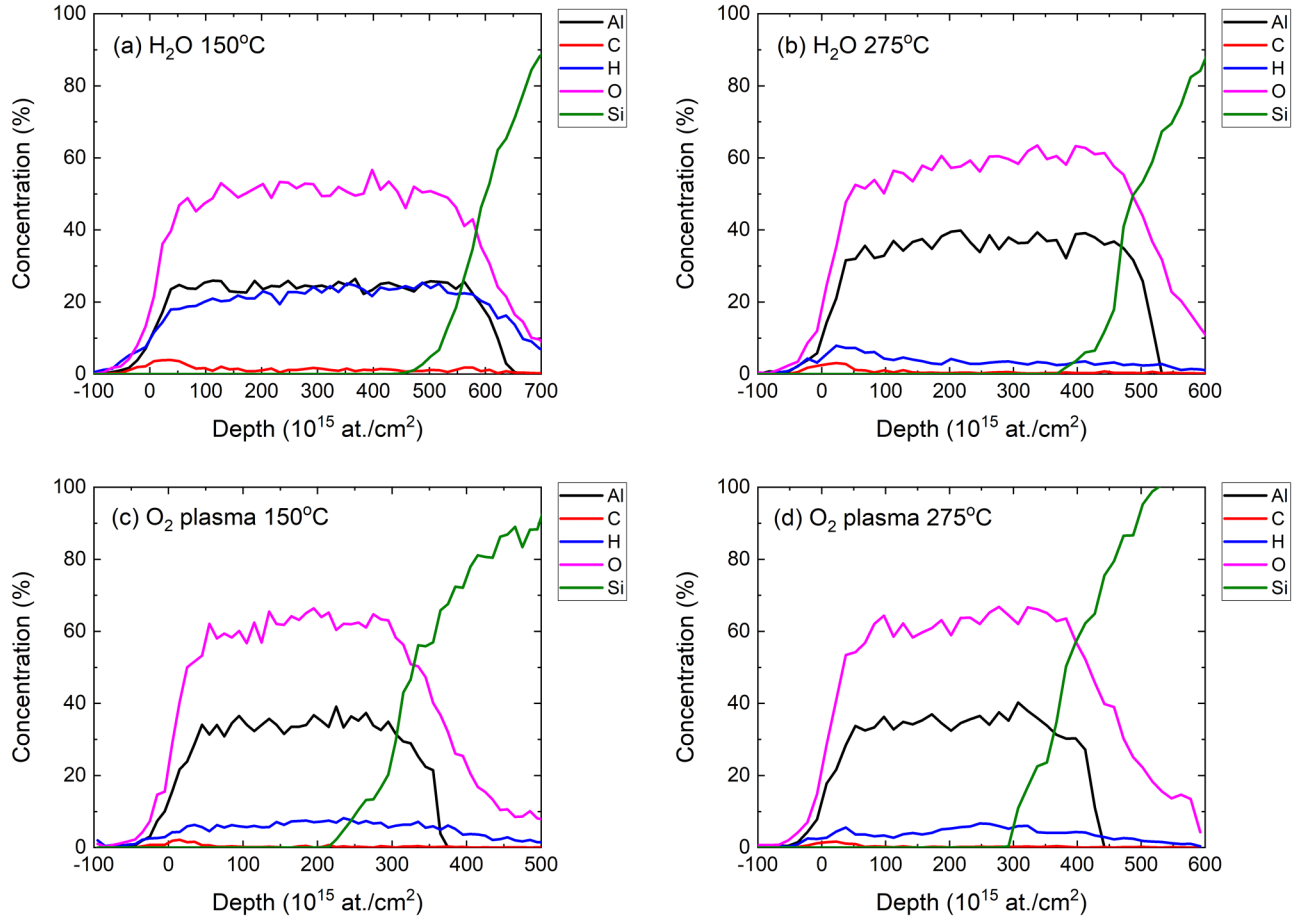

FIG. 4. ToF-ERD depth profiles of the four samples under study: H_2O ALD at (a) 150 °C and (b) 275 °C and O_2 PE-ALD at (c) 150 °C and (d) 275 °C.

PE-ALD process. Figure 4 shows the ToF-ERD depth profiles of these four samples. From an oxygen point of view, these high-density alumina films, i.e., PE-ALD and high-temperature thermal ALD, possess a stoichiometry close to that expected for Al_2O_3: 60 at. % O. However, the Al content is slightly lower than expected from a stoichiometric point of view (40 at. %) and does not reach 40 at. % even within the margin of error. Some H is present in these high-density films, between 3.1 at. % for the high-temperature thermal ALD and 4–6.1 at. % for the PE-ALD films. The presence of hydrogen in these films can originate from either precursor fragments built into the films, incorporated nonreacted OH groups or H_2O built into or absorbed into the layers. The first hypothesis is very unlikely due to the low C-content, while the incorporation of precursor ligands is expected to result in a 1:3 ratio of C:H. This leads to believe that either some OH groups are built into these films or water is present in the films. Assuming that alumina is present as Al_2O_3, atomic ratios of 2:3 are expected. When this ratio is corrected for the presence of OH groups, based on the measured H, in these three high-density cases, the Al:O ratio indeed approaches that of stoichiometric Al_2O_3. However, for the low-temperature water-based ALD films, i.e., the low-density films, this is not the case. Here, much higher H concentrations are detected, up to 24 at. %, which is staggeringly high for an ALD film at these deposition temperatures, but is commonly observed for near-room-temperature thermal ALD of Al_2O_3 using TMA.[45]

There are two hypotheses for explaining the origin of the high concentration of H at low temperature. One is to assume that Al is mainly present in the films in the form of Al_2O_3. In that case, the off-stoichiometry of the Al:O ratio can be corrected when built-in water (H/O: ½) is considered to be present in the film. This significant amount of water in the films can be built-in either from the deposition process as crystal water or soaked in postdeposition when these films were exposed to air. However, it is also possible to assume that the impurities are in the form of −OH groups and Al is present partly in the form of AlOOH. Similar film compositions have been reported when low-temperature deposition of alumina was performed using TIPA in a CVD process.[46] The presence of water and hydroxyl groups in the films can explain the low densities observed in these films. This distinction to the origin of hydrogen is an important differentiation to make, as the "solid" incorporation of −OH groups could be potentially relevant for applications in solar cells, where hydrogen could be used to passivate interface traps in the silicon, while the "liquid" incorporation of hydrogen in the form of water is not expected to cause this desired effect, and would need to be investigated in-depth for functional films in these applications.

To further investigate the characteristics of Al_2O_3 films deposited by TIPA precursor, the films were used as

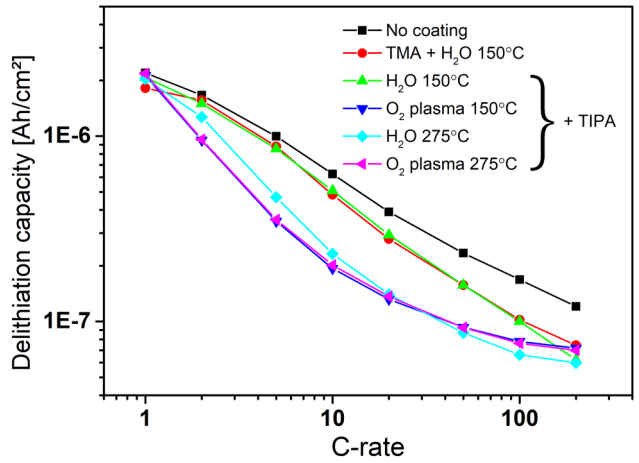

FIG. 5. Peukert plots of alumina coated TiO_2 electrodes.

amorphous coatings on a planar thin film Li-ion battery electrode. ALD Al_2O_3 has been extensively studied as a protective coating on battery materials, which often induces improved performance by suppressing solid electrolyte interface (SEI) formation, preventing metal dissolution and redeposition, maintaining electrode morphology, forming an artificial SEI layer, or scavenging HF.[47–52] However, as was highlighted in detail by Mattelaer *et al.*, Al_2O_3 also inevitably impedes battery kinetics due to the very high resistivity of ALD Al_2O_3 toward lithium ion transfer.[53] The exact nature and quality of the Al_2O_3 films, i.e., purity and density, could have a great influence on the exact nature of this added impedance.

In this work, ALD Al_2O_3 was acting as a buffer layer, imposing a kinetic bottleneck on a battery system and degrading the power capability of the electrode. Thin-film anatase TiO_2 was selected as the electrode because of its low volume change, zero metal dissolution, and electrochemical potential higher than solvent reduction potentials. Al_2O_3 films were deposited by the TIPA thermal ALD process and by the oxygen plasma ALD process at 150 and 275 °C. An Al_2O_3 film deposited by TMA and water at 150 °C was also used as a reference coating. The thickness of all films was 1.5 nm, and the coatings were deposited on 40 nm of anatase TiO_2, which is an ideal model material for investigating the influence of coated films on the kinetics of the electrode.[53] The coated electrodes were charged and discharged at different C-rates from 1C to 200C. A C-rate of 1C corresponds to a current density equivalent to charging the theoretical capacity of 40 nm TiO_2 in 1 h, while a C-rate of 200C corresponds

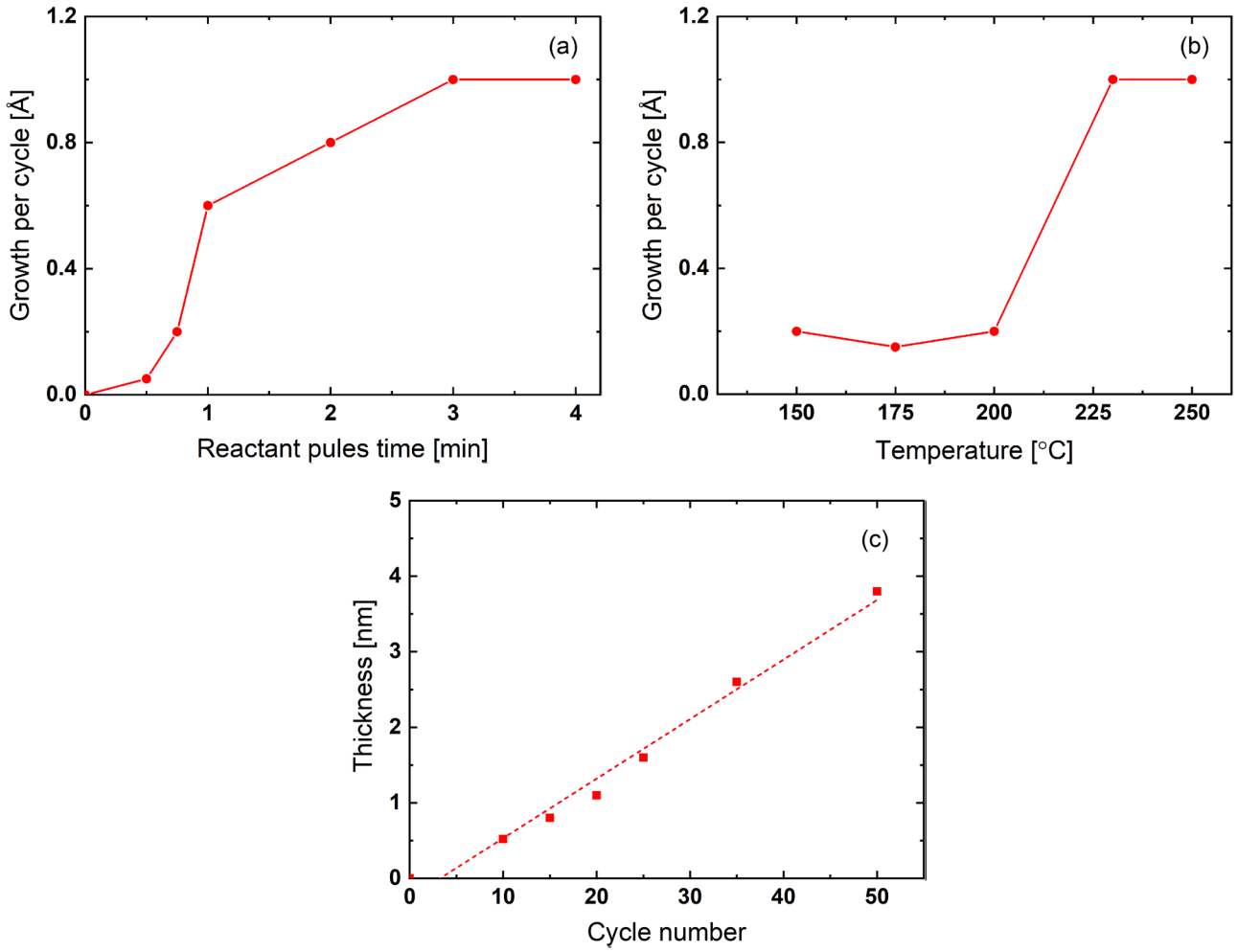

FIG. 6. (a) Saturation curve at 250 °C, (b) temperature window with saturated TIPA pulse (3 min), and (c) linear growth behavior of atmospheric pressure ALD on Si with TIPA pulse (3 min) and water pulse (40 s) at 250 °C.

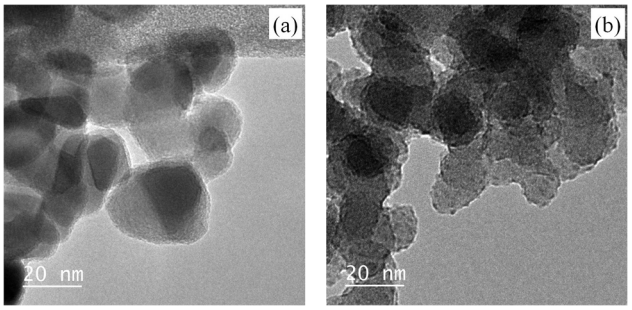

FIG. 7. TEM images of alumina deposited on Au grids containing (a) TiO_2 and (b) SiO_2 nanoparticles.

to a current density equivalent to charging the theoretical capacity of 40 nm TiO_2 in 1/200th of an hour, i.e., in 18 s. The applied current for each C-rate was calculated from the theoretical capacity for TiO_2 (168 mA h g^{-1}), the density for bulk anatase TiO_2 (3.78 g cm^{-3}), the cell surface (0.9503 cm^2), and the electrode thickness (40 nm). The theoretical capacity is 2.4 μA h; thus, the applied currents ranged from 2.4 μA (for 1C) to 480 μA (for 200C).

By analyzing the effect of coating on the kinetics, the quality of the different alumina ALD films was assessed. The Peukert plots, ranging from 1C to 200C, show the results for Al_2O_3 coated electrodes (Fig. 5). As recently reported by Mattelaer *et al.*, the Al_2O_3 coatings have a negative effect on the kinetics,[53] as is evident when comparing to the data for the uncoated TiO_2 reference electrode. The alumina film deposited at 150 °C by the TIPA thermal process shows a similar effect as the coating of the TMA thermal process film. This is a rather surprising result, given the high hydrogen content of the TIPA film. However, the conditions of battery cycling, i.e., submerging the films into a liquid battery electrolyte consisting of a lithium salt and a solvent, as well as lithium transfer across the alumina interface, may very well consume the hydrogen or water during initial battery testing, rendering these films in density and composition very close to the TMA thermal process film properties. Furthermore, the results also confirm that the alumina film deposited by O_2 plasma and by water at 275 °C more strongly reduces the kinetics of the buried TiO_2 electrode. This could be related to the higher film density and lower H concentration of these films.

Thermal ALD of TIPA and water operated in AP-ALD was first tested on flat Si substrates. TIPA saturation at 250 °C was achieved after 3 min pulse time reaching a growth of 1.1 Å/cycle [Fig. 6(a)]. This saturation time is longer than the TMA saturation in AP-ALD, as expected by the lower vapor pressure of TIPA compared to TMA. Two different ALD windows are observed for deposition of alumina, first between 150 and 200 °C with a growth of 0.2 Å/cycle and second at above 200 °C with a growth of 1.1 Å/cycle [Fig. 6(b)]. No growth was observed when ozone was used as the reactant. The deposition thickness on Si at 250 °C exhibits linear dependency on the number of ALD cycles [Fig. 6(c)]. XPS analysis on Si substrates shows a stoichiometric alumina deposition with no residual carbon in the film (Fig. 5 in the supplementary material[62]).

Deposition of alumina during the thermal water ALD is expected to happen due to the known facile reaction of alkoxides with hydroxyl groups.[54,55] *In situ* mass spectrometry analysis in the AP-ALD system shows the appearance of isopropanol upon pulsing water into the reactor after TIPA pulse (Fig. 6 in the supplementary material[62]).[56] Moreover, the absence of propene peaks confirms that the deposition is not happening via precursor decomposition.[57] This suggests that a possible mechanism for the reaction of water with the adsorbed TIPA molecule and deposition of Al_2O_3 is via the following equation:

$$2Al(OCH(CH_3)_2)_3 + 3H_2O \rightarrow Al_2O_3 + 6(CH_3)_2CHOH. \quad (1)$$

However, recent results from density functional theory simulations suggest that possibly not all ligands are removed in the same manner.[44] The computational data and the *in situ* mass spectrometry analysis both confirm that the formation of the alumina film mainly occurs during the water pulse by ligand exchange reactions between water and adsorbed precursors.

To further investigate the potential of using TIPA as a precursor for large-scale applications, we performed thermal AP-ALD on small amounts of nanoparticles coated on Au

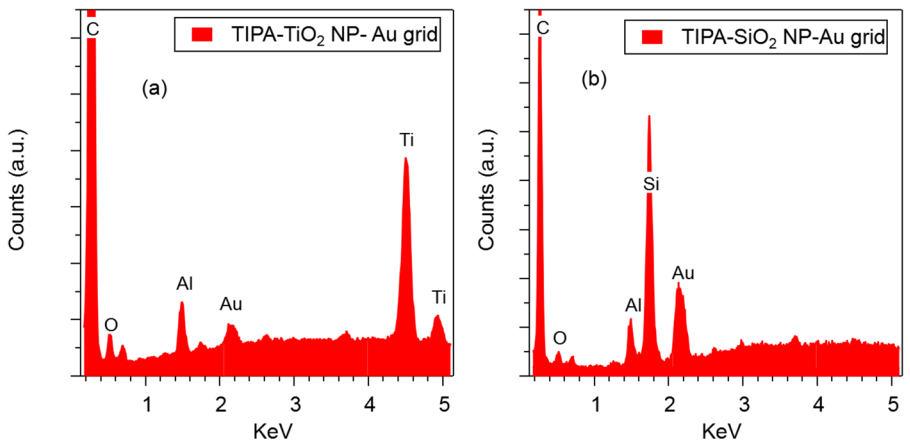

FIG. 8. EDX-TEM analysis on alumina coated TEM grids containing (a) TiO_2 and (b) SiO_2 nanoparticles.

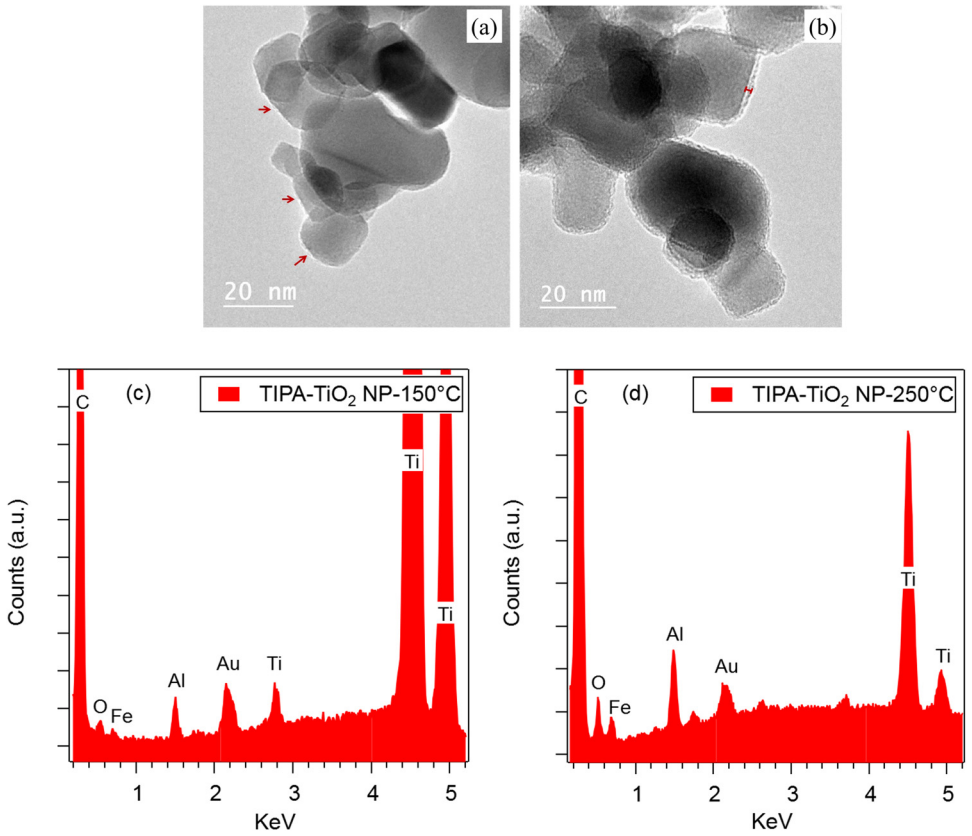

FIG. 9. (a) TEM and (c) EDX analysis of TiO_2 nanoparticles coated at 150 °C (arrows indicate where the deposition has started), (b) TEM and (d) EDX analysis of TiO_2 nanoparticles coated at 250 °C (marker shows a thin film with a thickness of approximately 1.1 nm).

TEM grids. We chose TiO_2 and SiO_2 as the candidates for the deposition of alumina due to their applications as support material in photocatalysis, paint, and biomedical industry.[58–61] For these experiments, small amounts of nanoparticles (in the order of milligram) are dispersed in ethanol and drop-casted on Au TEM grids. The solvent is then evaporated and the grids containing the nanoparticles are transferred into the ALD chamber for deposition of alumina. The deposition was done at 150 °C for 25 cycles under saturation behavior for TIPA (3 min pulse time). TEM results confirm the deposition of alumina on TiO_2 nanoparticles in the form of thin films [Fig. 7(a)] and on SiO_2 nanoparticles in the form of islands [Fig. 7(b)]. Due to the different surface properties of these nanoparticles, different deposition behaviors can be expected. TiO_2 surface has more than twice the number of hydroxyl groups compared to SiO_2 surface allowing for a different form of reaction between the precursor molecules and the available surface groups.

EDX-TEM analysis done on the nanoparticles confirms the deposition of alumina on both substrates with up to approximately 1.5% Al present on the samples (Fig. 8). The strong C signal observed in these spectra is mostly contributed from the carbon mesh on the TEM grids. Other small peaks present in the spectrum include Au, Cu, and Fe and originate from the TEM grid and the TEM background environment.

Next, the process was scaled-up to larger amounts of nanoparticles. For this purpose, a 1 g batch of nanoparticles was fluidized in the AP-ALD system. The surface area for this amount of TiO_2 nanoparticles is 52.4 m^2. As the surface area of 1 g of nanoparticles is more than 1000 times larger than the surface area of typical solid substrates, when investigating industrial applications of ALD on nanoparticles, much longer pulse times are required for achieving saturation. ALD of alumina was performed on the particles at 150 and 250 °C with a TIPA pulse time of 30 min and 10 min water pulse. Upon ten cycles of ALD performed at 150 °C, some roughening of the nanoparticles and formation of thin alumina films start to appear, but the deposited film is too thin to be detected by TEM [Fig. 9(a)]. EDX-TEM analysis of the nanoparticles confirms the presence of an average amount of 0.8 wt. % Al on this sample [Fig. 9(c)]. Performing the same number of ALD cycles on nanoparticles at 250 °C results in deposition of a uniform thin film of approximately 1 nm thick [Fig. 9(b)] and an increased average amount of Al in EDX-TEM (2.1 wt. %) [Fig. 9(d)]. The difference in growth rates is in agreement with the observations on flat substrates where growth per cycle at 150 °C was lower than 250 °C.

IV. SUMMARY AND CONCLUSIONS

We have shown the use of TIPA for the deposition of alumina on flat substrates (surface area: cm^2) and on nanoparticles (surface area: m^2). Thermal water ALD in vacuum and atmospheric pressure systems showed growth windows

of 125–300 °C and 150–250 °C, respectively, with growth rates higher than or similar to the TMA thermal process. No growth was observed in both systems when ozone was used as the reactant. Plasma-assisted ALD using water and oxygen plasma showed growth rates of 1.1 Å/cycle. Studies on nanoparticles confirm the growth on small amounts (milligram) of TiO_2 and SiO_2 nanoparticles. Moreover, alumina growth is observed when larger batches (gram) of TiO_2 nanoparticles with a total surface area of about 52 m^2 are used. While the vapor pressure of TIPA is lower than TMA and deposition of alumina using TIPA requires higher deposition temperatures compared to the TMA process, this precursor has the potential to be used on large surfaces and for applications where safety issues prohibit the use of pyrophoric precursors like TMA. Using TIPA as a precursor for ALD would open up the possibility of coating large areas at moderate temperatures for applications outside of the cleanroom such as photovoltaics and powder coating.

ACKNOWLEDGMENTS

This work is supported by the M-ERA CALDERA project, the Fund for Scientific Research Flanders (FWO), and the Dutch Research Council (NWO). Timo Hatanpää (University of Helsinki) performed TGA measurements and vapor pressure calculations of TIPA.

[1]Y. Liu, J. Tolentino, M. Gibbs, R. Ihly, C. L. Perkins, Y. Liu, N. Crawford, J. C. Hemminger, and M. Law, Nano Lett. **13**, 1578 (2013).
[2]S. ten Cate, Y. Liu, C. S. Suchand Sandeep, S. Kinge, A. J. Houtepen, T. J. Savenije, J. M. Schins, M. Law, and L. D. A. Siebbeles, J. Phys. Chem. Lett. **4**, 1766 (2013).
[3]D. Valdesueiro *et al.*, J. Phys. Chem. C **120**, 4266 (2016).
[4]S. Jakschik, U. Schroeder, T. Hecht, G. Dollinger, A. Bergmaier, and J. W. Bartha, Mater. Sci. Eng. B **107**, 251 (2004).
[5]P. Poodt, A. Lankhorst, F. Roozeboom, K. Spee, D. Maas, and A. Vermeer, Adv. Mater. **22**, 3564 (2010).
[6]S. Dueñas *et al.*, J. Appl. Phys. **99**, 054902 (2006).
[7]W. M. M. Kessels and M. Putkonen, MRS Bull. **36**, 11 (2011).
[8]D. Longrie, D. Deduytsche, and C. Detavernier, J. Vac. Sci. Technol. A **32**, 010802 (2013).
[9]H. Van Bui, F. Grillo, and J. R. van Ommen, Chem. Commun. **53**, 45 (2017).
[10]E. Granneman, P. Fischer, D. Pierreux, H. Terhorst, and P. Zagwijn, Surf. Coat. Technol. **201**, 22 (2007).
[11]S. M. George, A. W. Ott, and J. W. Klaus, J. Phys. Chem. **100**, 13121 (1996).
[12]M. Leskelä and M. Ritala, Thin Solid Films **409**, 138 (2002).
[13]L. Markku and R. Mikko, Angew. Chem. Int. Ed. **42**, 5548 (2003).
[14]R. L. Puurunen, J. Appl. Phys. **97**, 12 (2005).
[15]S. M. George, Chem. Rev. **110**, 111 (2010).
[16]V. Miikkulainen, M. Leskelä, M. Ritala, and R. L. Puurunen, J. Appl. Phys. **113**, 021301 (2013).
[17]J. A. McCormick, B. L. Cloutier, A. W. Weimer, and S. M. George, J. Vac. Sci. Technol. A **25**, 67 (2007).
[18]W. Cho, K. Sung, K.-S. An, S. S. Lee, T.-M. Chung, and Y. Kim, J. Vac. Sci. Technol. A **21**, 1366 (2003).
[19]S. E. Potts, G. Dingemans, C. Lachaud, and W. M. M. Kessels, J. Vac. Sci. Technol. A **30**, 021505 (2012).
[20]A. L. Brazeau and S. T. Barry, Chem. Mater. **20**, 23 (2008).
[21]M. Ritala, H. Saloniemi, M. Leskelä, T. Prohaska, G. Friedbacher, and M. Grasserbauer, Thin Solid Films **286**, 54 (1996).
[22]S. J. Yun, K.-H. Lee, J. Skarp, H.-R. Kim, and K.-S. Nam, J. Vac. Sci. Technol. A **15**, 2993 (1997).
[23]M. Tiitta, E. Nykänen, P. Soininen, L. Niinistö, M. Leskelä, and R. Lappalainen, Mater. Res. Bull. **33**, 1315 (1998).
[24]G.-I. Oya and Y. Sawada, J. Cryst. Growth **99**, 1 (1990).
[25]R. Huang and A. H. Kitai, J. Electron. Mater. **22**, 215 (1993).
[26]K. Kukli, M. Ritala, M. Leskelä, and J. Jokinen, J. Vac. Sci. Technol. A **15**, 2214 (1997).
[27]S. Blittersdorf, N. Bahlawane, K. Kohse-Höinghaus, B. Atakan, and J. Müller, Chem. Vap. Deposition **9**, 194 (2003).
[28]A. N. Gleizes, C. Vahlas, M. M. Sovar, D. Samélor, and M. C. Lafont, Chem. Vap. Deposition **13**, 23 (2007).
[29]J. A. Aboaf, J. Electrochem. Soc. **114**, 948 (1967).
[30]M. Ritala, K. Kukli, A. Rahtu, P. I. Räisänen, M. Leskelä, T. Sajavaara, and J. Keinonen, Science **288**, 319 (2000).
[31]L. Hiltunen, H. Kattelus, M. Leskelä, M. Mäkelä, L. Niinistö, E. Nykänen, P. Soininen, and M. Tiittad, Mater. Chem. Phys. **28**, 379 (1991).
[32]D. C. Bradley, Nature **182**, 1211 (1958).
[33]V. J. Shiner, D. Whittaker, and V. P. Fernandez, J. Am. Chem. Soc. **85**, 2318 (1963).
[34]G. P. Shulman, M. Trusty, and J. H. Vickers, J. Org. Chem. **28**, 907 (1963).
[35]W. Fieggen and H. Gerding, Recl. Trav. Chim. Pays-Bas **89**, 2 (1970).
[36]R. H. T. Bleyerveld, W. Fieggen, and H. Gerding, Recl. Trav. Chim. Pays-Bas **91**, 477 (1972).
[37]T. Dobbelaere, F. Mattelaer, A. K. Roy, P. Vereecken, and C. Detavernier, J. Mater. Chem. A **5**, 330 (2017).
[38]A. Goulas and J. Ruud van Ommen, J. Mater. Chem. A **1**, 4647 (2013).
[39]M. Laitinen, M. Rossi, J. Julin, and T. Sajavaara, Nucl. Instrum. Methods Phys. Res. Sect. B **337**, 55 (2014).
[40]K. Arstila, J. Julin, M. I. Laitinen, J. Aalto, T. Konu, S. Kärkkäinen, S. Rahkonen, M. Raunio, J. Itkonen, J. P. Santanen, T. Tuovinen, and T. Sajavaara, Nucl. Instrum. Methods Phys. Res., Sect. B **331** (2014).
[41]R. C. Wilhoit, J. Phys. Chem. **61**, 114 (1957).
[42]M. M. Sovar, D. Samélor, A. N. Gleizes, and C. Vahlas, Surf. Coat. Technol. **201**, 9159(2007).
[43]A. W. Ott, K. C. McCarley, J. W. Klaus, J. D. Way, and S. M. George, Appl. Surf. Sci. **107**, 128 (1996).
[44]T. B. Tai, L. Cao, F. Mattelaer, G. Rampelberg, F. S. M. Hashemi, J. Dendooven, J. R. van Ommen, C. Detavernier, and M. F. Reyniers, J. Phys. Chem. C **123**, 1 (2019).
[45]M. D. Groner, F. H. Fabreguette, J. W. Elam, and S. M. George, Chem. Mater. **16**, 639 (2004).
[46]P.-L. Etchepare, L. Baggetto, H. Vergnes, D. Samélor, D. Sadowski, B. Caussat, and C. Vahlas, Phys. Status Solidi C **12**, 944 (2015).
[47]Y. S. Jung, A. S. Cavanagh, L. A. Riley, S.-H. Kang, A. C. Dillon, M. D. Groner, S. M. George, and S.-H. Lee, Adv. Mater. **22**, 2172 (2010).
[48]J.-T. Lee, F.-M. Wang, C.-S. Cheng, C.-C. Li, and C.-H. Lin, Electrochim. Acta **55**, 4002 (2010).
[49]L. A. Riley, A. S. Cavanagh, S. M. George, Y. S. Jung, Y. Yan, S.-H. Lee, and A. C. Dillon, ChemPhysChem **11**, 2124 (2010).
[50]L. A. Riley, S. Van Atta, A. S. Cavanagh, Y. Yan, S. M. George, P. Liu, A. C. Dillon, and S.-H. Lee, J. Power Sources **196**, 3317 (2011).
[51]L. Jian and S. Xueliang, Nanotechnology **26**, 024001 (2015).
[52]B. Ahmed, C. Xia, and H. N. Alshareef, Nano Today **11**, 250 (2016).
[53]F. Mattelaer, P. M. Vereecken, J. Dendooven, and C. Detavernier, Adv. Mater. Interfaces **4**, 1601237 (2017).
[54]R. C. Mehrotra, J. Non-Cryst. Solids **121**, 1 (1990).
[55]M. Ritala, M. Leskela, L. Niinisto, and P. Haussalo, Chem. Mater. **5**, 1174 (1993).
[56]K. Knapas and M. Ritala, Crit. Rev. Solid State Mater. Sci. **38**, 167 (2013).
[57]A. Rahtu and M. Ritala, Chem. Vap. Deposition **8**, 1 (2002).
[58]H. Shi, R. Magaye, V. Castranova, and J. Zhao, Part. Fibre Toxicol. **10**, 1 (2013).
[59]A. Bitar, N. M. Ahmad, H. Fessi, and A. Elaissari, Drug Discov. Today **17**, 1147 (2012).
[60]Y. Wang *et al.*, Nanomedicine **11**, 313 (2015).
[61]Y. Bessekhouad, D. Robert, and J. V. Weber, J. Photochem. Photobiol. A **157**, 47 (2003).
[62]See supplementary material at https://doi.org/10.1116/1.5093402 for data on vapor pressure of precursor, GPC versus precursors purge time, oxidizer saturation curve, XPS analysis, and *in situ* mass spectrometry.